J. Fluid Mech. (1984), *vol.* 139, *pp.* 417–434
Printed in Great Britain

LDV measurements of an air–solid two-phase flow in a vertical pipe

By YUTAKA TSUJI, YOSHINOBU MORIKAWA AND HIROSHI SHIOMI

Faculty of Engineering, Osaka University, Osaka, Japan

(Received 25 April 1983)

Measurements of air and solid-particle velocities were made in a vertical pipe two-phase flow by the use of a laser-Doppler velocimeter (LDV). Five kinds of plastic particles, diameters of which ranged from about 3 mm to 200 μm, were transported in a vertical pipe of 30 mm inner diameter. It was found that, the smaller the particle size, the flatter was the mean air velocity distribution for the same mass flow ratio of solids to air. Large particles increased air turbulence throughout the pipe section, while small particles reduced it. Both effects of promotion and suppression of turbulence were observed at the same time in the presence of particles of medium size, that is, the turbulence was increased around the pipe centre and reduced near the wall. The frequency spectrum of air turbulence normalized by the turbulence intensity was not changed by the large particles. In the presence of the small particles, the higher-frequency parts of the spectrum increased.

1. Introduction

We have previously (Tsuji & Morikawa 1982) made measurements of an air–solid two-phase flow by the use of LDV (laser–Doppler velocimeter). In that work, two kinds of plastic particles, the mean diameters of which were 3.4 and 0.2 mm respectively, flowed in a horizontal pipe. Small tracers of ammonium chloride were also seeded in the flow for detecting the motion of the air phase. LDV signals of the air phase were extracted by an electronic device making use of the different characteristics of the air and solid phases. Tsuji & Morikawa (1982) showed that the particles changed the distributions of intensity and spectrum of air turbulence. The present work is an extension of the previous one, investigating the case of a vertical pipe.

Asymmetric structure due to gravity is inevitable in a horizontal pipe, which makes the flow mechanism more complicated than in a vertical pipe. One can get rid of such a kind of asymmetric structure in the vertical pipe and hence observe the phenomena in a simple manner. In this experiment, effects of particle size were investigated more systematically by using particles of various sizes.

2. Experimental equipment and method

2.1. *Pipeline*

Figure 1 shows the experimental rig. The air was supplied by a turbo-blower (10) and passed the flow measuring section (7) incorporating a Pitot tube. A part of the air passed into a smoke-generating chamber (12), which provided tracer particles for the air

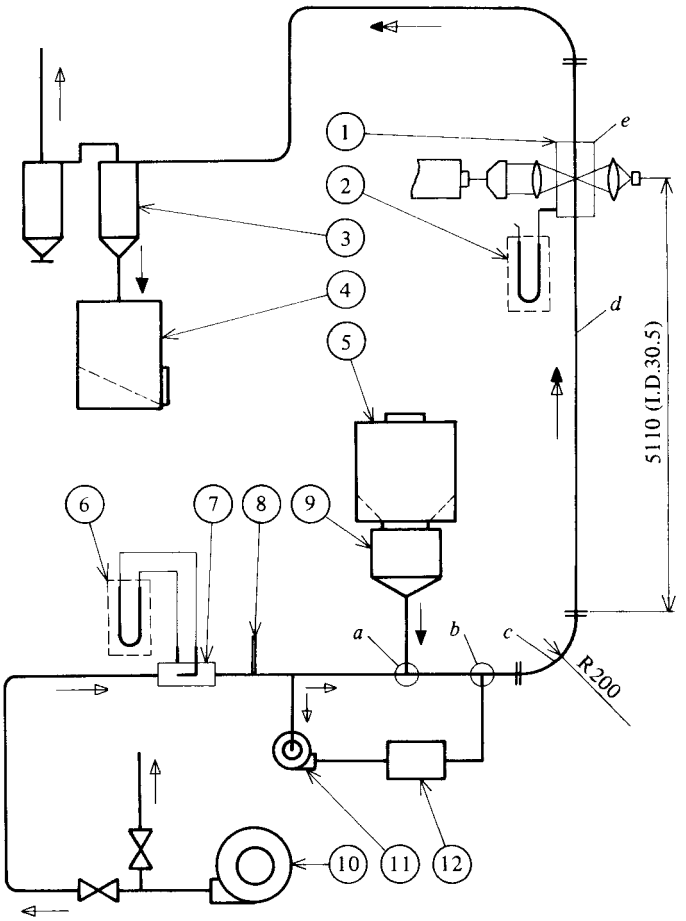

FIGURE 1. Experimental pipeline: 1, LDV test section; 2, manometer; 3, cyclone separator; 4, solid receiver; 5, solid storage chamber; 6, manometer, 7, measuring section of air-flow rate; 8, thermometer; 9, electromagnetic feeder; 10, blower; 11, supercharger; 12, smoke generator.

Number	1	2	3	4	5
Particle type	cylindrical particle	3 mm particle	1 mm particle	500 m particle	200 m particle
Material	polyethylene	polystyrene	polystyrene	polystyrene	polystyrene
Shape	short cylinder	sphere	sphere	sphere	sphere
Mean volume diameter	3.43 mm	2.78 mm	1.42 mm	501 m	243 m
Density (kg/m^3)	970	1020	1030	1020	1020

TABLE 1. Properties of test particles

phase, and returned to the main pipe. The air was mixed with test particles at the particle-feeding point, passed a horizontal–vertical bend c and was supplied to the vertical test section ① (inner diameter $D = 30.5$ mm) as a two-phase flow. The internal diameter of the bend was 40 mm and the radius of curvature was 200 mm. The pipe diameter changed abruptly at the bend outlet from 40 to 30.5 mm. The particles

sliding on the bend outer wall owing to the centrifugal force were dispersed owing to the above stepwise decrease in diameter. Therefore there was no effect of the bend on the particle distributions in the test section. A number of static pressure taps were set up along the vertical pipe. The test section was made of a glass pipe of 0.9 mm thickness. The distance between the bend outlet and the test section was 5110 mm, which was long enough to confirm that the particle motion reached a steady state at the test section.

Five kinds of plastic pellets were used in the experiment. Their properties are shown in table 1. These particles were supplied to the pipeline by an electromagnetic feeder ⑨ and separated from air by a cyclone separator ③. When plastic particles are repeatedly conveyed pneumatically, electrostatic charging caused by friction between the particles and pipe wall is marked, especially for small particles. To prevent the effects of charging, the particles of 200 μm and 500 μm diameter were coated with a charge-preventing substance which is commercially available for use on clothes. Tracer particles for detecting the air flow were ammonium chloride smoke of mean diameter 0.6 μm. The concentration of the smoke was adjusted to such a height that the spectrum of the tracker output compared well with that of a hot-wire anemometer up to several kHz in a single-phase flow. In this experiment, the mean air velocity $\bar{u}_m$ ranged from 8 to 20 m/s and the loading ratio m defined as the particle-to-air mass-flow-rate ratio was up to 5.

LDV measurements in vertical pipes of other workers are cited in this paper for comparison, and therefore their experimental conditions are briefly mentioned. Maeda, Hishida & Furutani (1980) performed an experiment in pipes of 38 and 56 mm inner diameters, using three kinds of particles, namely 45 μm and 136 μm glass beads and 93 μm copper beads. The range of mean air velocities in their work was from 4.1 to 5.7 m/s and the loading ratios were less than 0.8. The experiment by Lee & Durst (1982) was conducted in a pipe of 42 mm inner diameter with the mean air velocity at 5.7 m/s, and four kinds of glass beads (100, 200, 400 and 800 μm) were used. The loading ratio ranged between about 1.5–3.0. Compared with the present work, the works mentioned above were made at low air velocities using particles of high densities.

2.2. *Optical arrangement and signal-processing system*

Since the optical arrangement and signal-processing system in this work is almost the same as in Tsuji & Morikawa (1982), only primary points are described here. A LDV was set up in a dual-beam forward-scattering mode with a 15 mW He–Ne laser and 100 mm focal-length lens. A frequency tracker converted the frequency of a Doppler burst signal into a voltage output proportional to the velocity. The Doppler signal was obtained not only from the small tracers but also from the spherical test particles. Therefore simultaneous measurements of velocities of both air and solid phases were made possible by making use of a specially designed signal-discrimination device. The principle of the signal discriminator is that the burst signals with sufficiently large pedestal components come from the large particles, while those with small pedestal but large Doppler components come from the small tracers that follow the fluid motion. Details of the use of this discriminator were described by Tsuji & Morikawa (1982). The discriminated signals from the tracker were stored once in an analog data recorder and were processed by a digital computer (FACOM M200) following an A/D-converter. Digitizing rates were 40 kHz.

Signal discrimination is not necessary when only the velocities of test particles are to be measured. Therefore an experiment without small tracers was also made, and

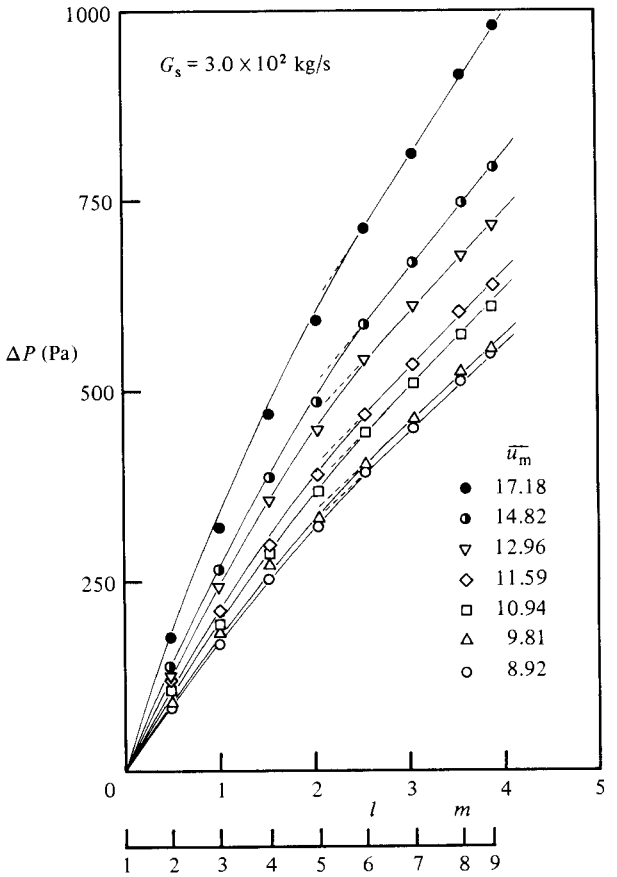

FIGURE 2. Pressure distribution in the presence of 500 μm particles (G_s = particle mass-flow rate).

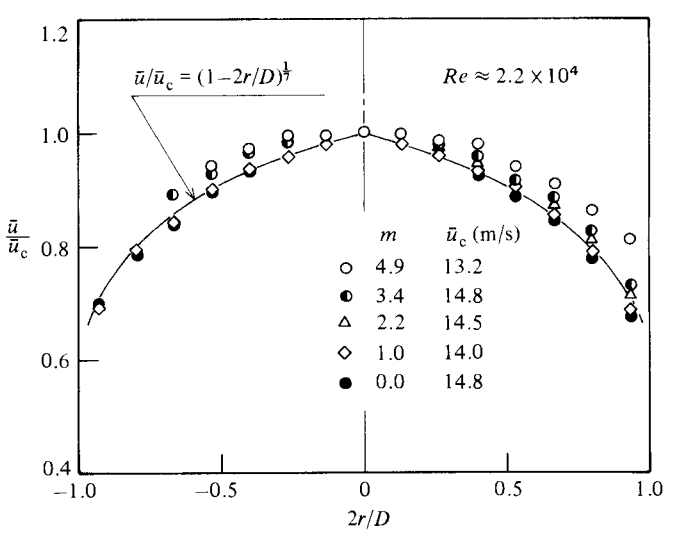

FIGURE 3. Mean air-velocity distribution in the presence of cylindrical particles.

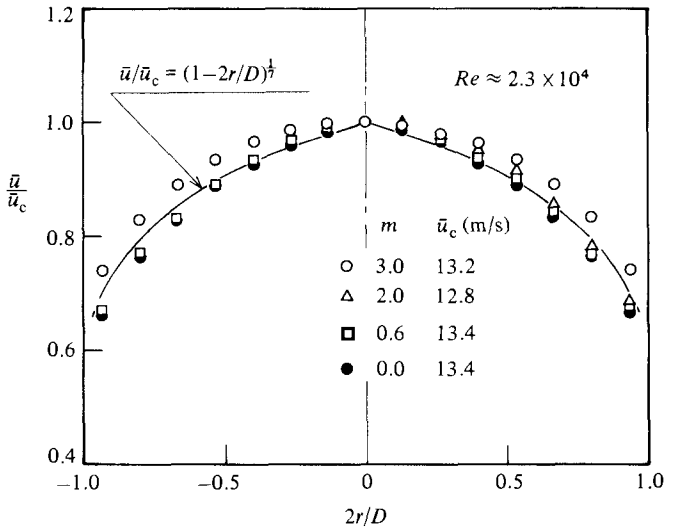

FIGURE 4. Mean air-velocity distribution in the presence of 1 mm particles.

the velocities of test particles were compared with the results from signal discrimination in the simultaneous measurements. It was confirmed that good agreement was obtained between both results.

3. Results

3.1. *Pressure drop*

Gas–solid two-phase flow in a pipe closely relates to pneumatic conveying technology of solid particles. In the field of pneumatic conveying, a great concern is the pressure drop. Figure 2 presents the pressure distribution along the vertical pipe with 500 μm particles conveyed, where the position of the bend outlet is chosen as the origin of abscissa. The particles that are decelerated in the bend are accelerated beyond the bend so that the pressure gradient is high near the bend. As the flow moves further downstream, the gradient gradually becomes constant. In the region of constant pressure gradient, particle velocities also reach constant values statistically, or in other words particle motion is in a steady state. The present test section was located at $l = 5110$ mm, and thus LDV measurements were made in the region of constant pressure gradient or velocity. The larger the particle size, the longer the distance for which the steady state of particle motion was assured. It was confirmed that the present test section was in the steady region for all kinds of particles used.

3.2. *Mean velocity*

Figures 3 and 4 show mean air-velocity distributions in the presence of relatively large particles, where the results of cylindrical pellets and 1 mm spheres are given with different loading ratios. In the figures $\bar{u}_c$ is the velocity at the pipe centre and r is the radial distance measured from the pipe centre. It is found that the velocity distributions are slightly flattened by the particles, but the effect of large particles is not so large within the present experimental condition. Figures 5 and 6 are the results for 500 and 200 μm particles. In spite of the same order of loading ratios as in figures 3 and 4, the effect of small particles on the distribution is remarkable

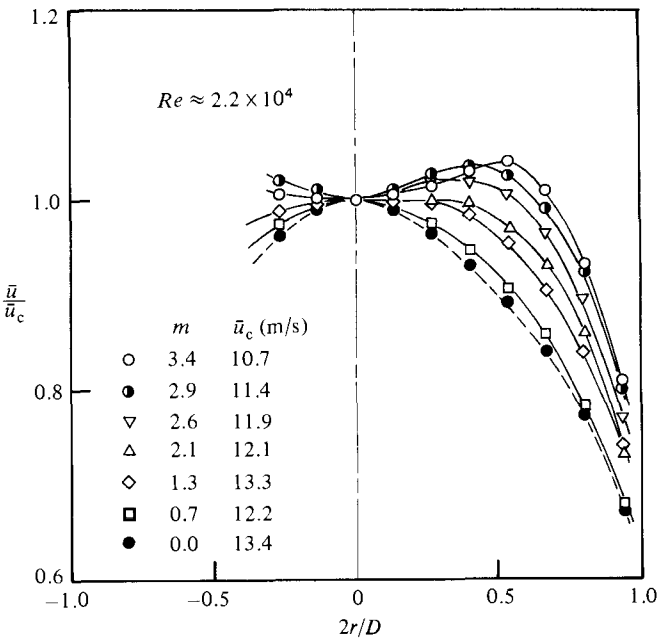

FIGURE 5. Mean air-velocity distribution in the presence of 500 μm particles.

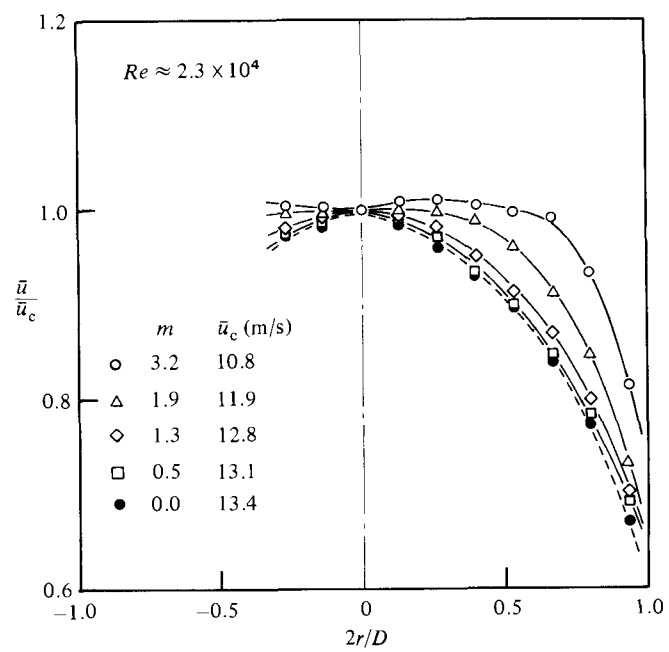

FIGURE 6. Mean air-velocity distribution in the presence of 200 μm particles.

in figures 5 and 6. Besides the flattening effect, the point of maximum velocity deviates from the pipe axis as the loading ratio increases, especially in the case of 500 μm particles. As a result, the velocity profile becomes concave. The distributions for 200 μm particles also show a slight similar trend. Such a concave profile was not reported in LDV measurements in a vertical pipe by others. However, experimental

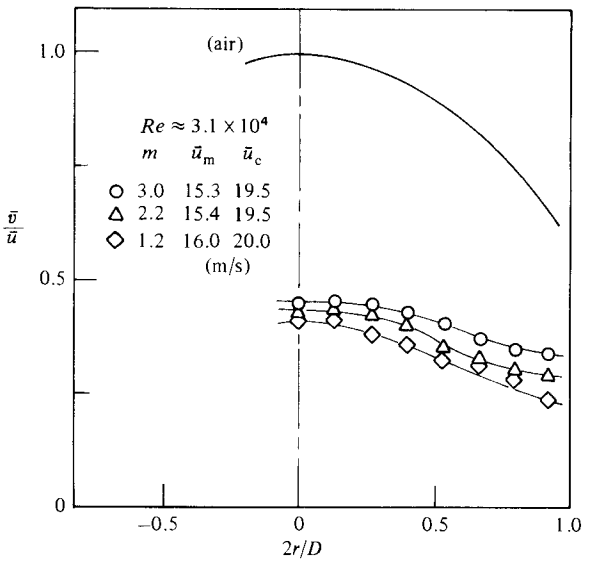

FIGURE 7. Mean air-velocity distribution in the presence of 3 mm particles.

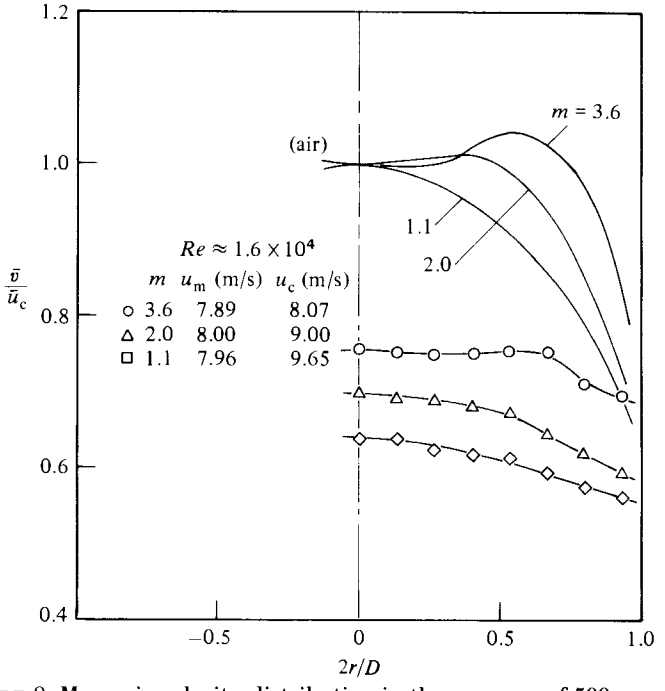

FIGURE 8. Mean air-velocity distribution in the presence of 500 μm particles.

results in a vertical pipe by Vollheim (1965), who measured the mean air velocity by a Pitot tube, showed markedly concave distributions in the presence of large particles but at high loading ratios (m = 1–17). Similar concave distributions were found in a horizontal pipe for 200 μm particles in Tsuji & Morikawa (1982).

Figures 7–9 show the distributions of mean particle velocities. The profiles of mean air velocities are shown in the figures for comparison, but the Reynolds numbers differ

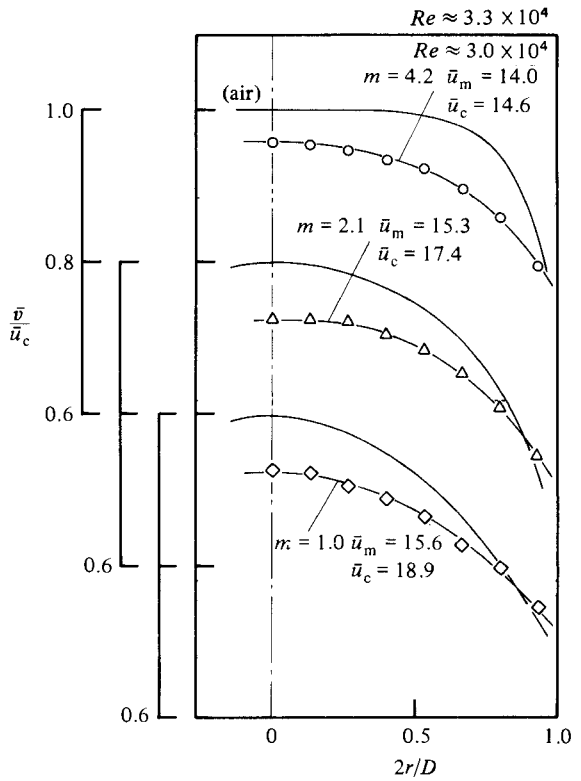

FIGURE 9. Mean particle-velocity distribution in the presence of 200 μm particles.

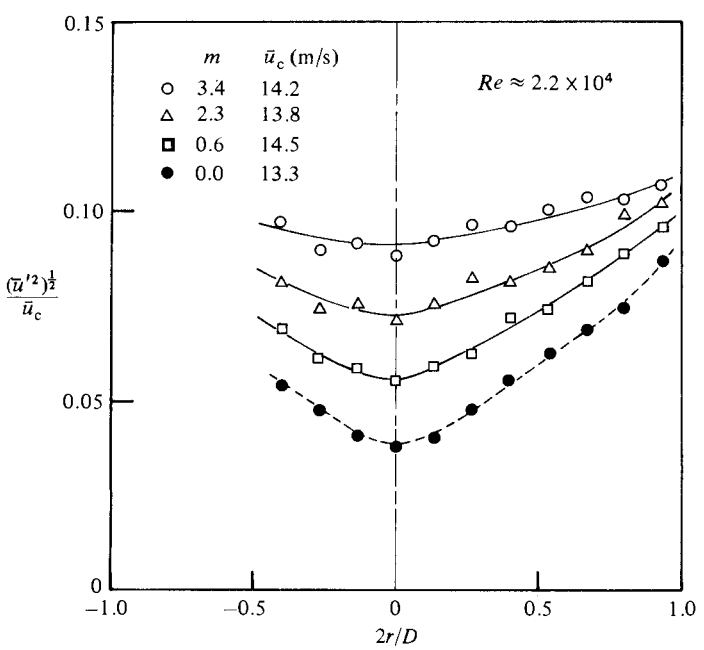

FIGURE 10. Turbulence intensity of air in the presence of 3 mm particles.

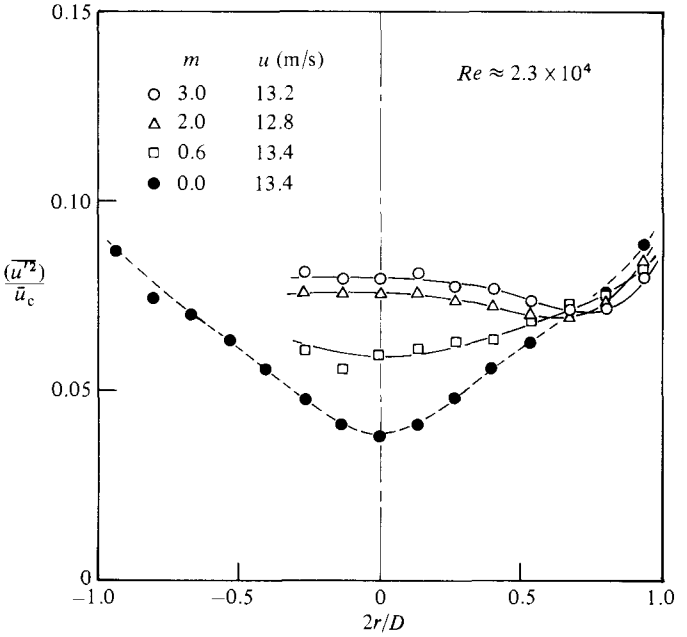

FIGURE 11. Turbulence intensity of air in the presence of 1 mm particles.

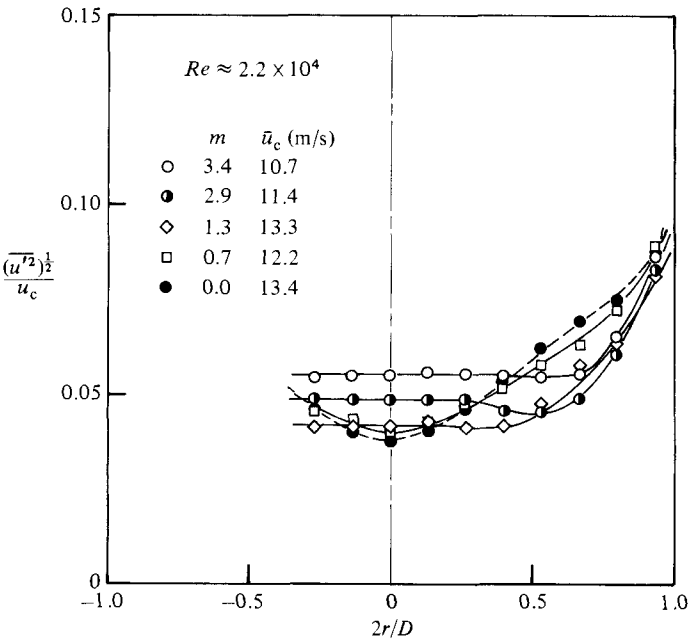

FIGURE 12. Turbulence intensity of air in the presence of 500 μm particles.

from those in figures 3–6 to avoid duplication. The distributions of particles are flat except for the case of 200 μm spheres, and the velocities increase with increasing loading ratios. The particle velocities are smaller than the air velocities in most parts of the pipe section, but they become larger than the air velocities near the wall because the air flow is subject to the viscous condition on the wall. Therefore, in a vertical

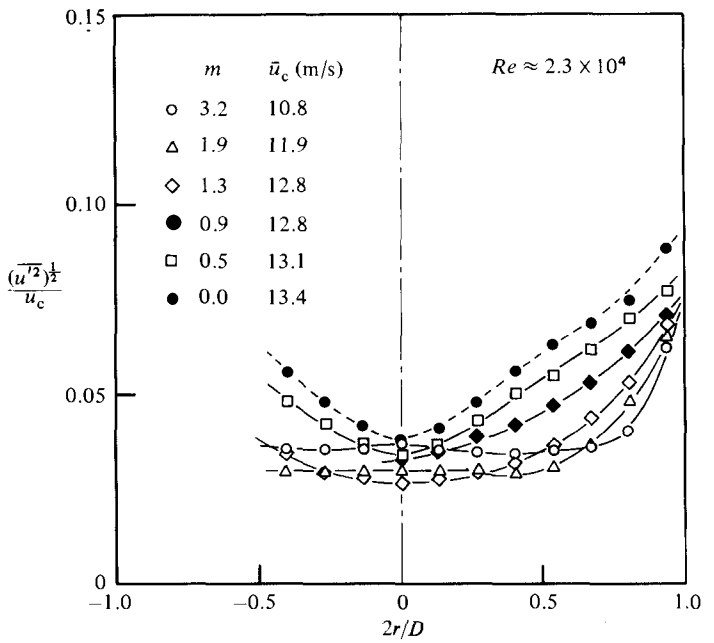

FIGURE 13. Turbulence intensity of air in the presence of 200 μm particles.

pipe flow, there must be a location where the sign of relative velocity between both phases changes. In general, the smaller the particle size, the less the value of the relative velocity. As a result, the change in sign occurs more easily for the small particles. For example, Lee & Durst (1982) showed that the distance of the change in sign from the wall was $0.1R$ for 200 μm glass beads and $0.2R$ for 100 μm glass beads, where R is the pipe radius. It was difficult in the present experiment to obtain the distance of the change in sign for particles other than 200 μm particles, because it was too close to the wall for other particles. As has been described, the particle velocities increase with increasing loading ratio, but at the same time the air-velocity profiles become flatter. Thus the location of the change in sign approaches the wall at high loading ratios as shown in figure 9.

Figures 10–13 show distributions of turbulence intensities $(\overline{u'^2})^{\frac{1}{2}}/\bar{u}_0$ of the air flow, where u' is the axial fluctuation component of air velocity. It is found that the air-flow turbulence is greatly influenced by the particles and the mode of influence differs with particle size. In the case of 3 mm particles, increase in turbulence is so remarkable that the distribution shows an almost uniform profile over the section at a high loading ratio. The results of the case of 1 mm particles are a little different from those of 3 mm particles. First, turbulence suppression is observed near the wall, though the turbulence increases considerably for most of the pipe section. In other words, two effects of particles, namely promotion and suppression of turbulence, appear in the same section. Secondly, the distribution is not monotone at relatively high loading ratios; that is, the intensities show minimum values around 0.6–$0.7R$. The results for 500 μm particles are qualitatively the same as those for 1 mm particles. However, the region of turbulence suppression spreads from near the wall to the pipe centre. 200 μm particles suppress the turbulence throughout the pipe section. Observing the change in intensity near the pipe centre in detail, the intensity that decreases at first with increasing loading ratio, increases again as the loading ratio

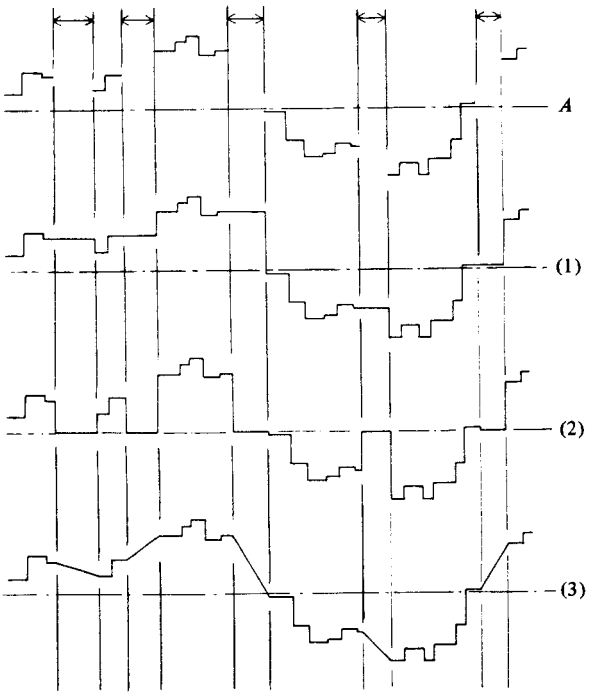

FIGURE 14. Simulation signals and interpolation scheme for defective parts: ↔, defective part.

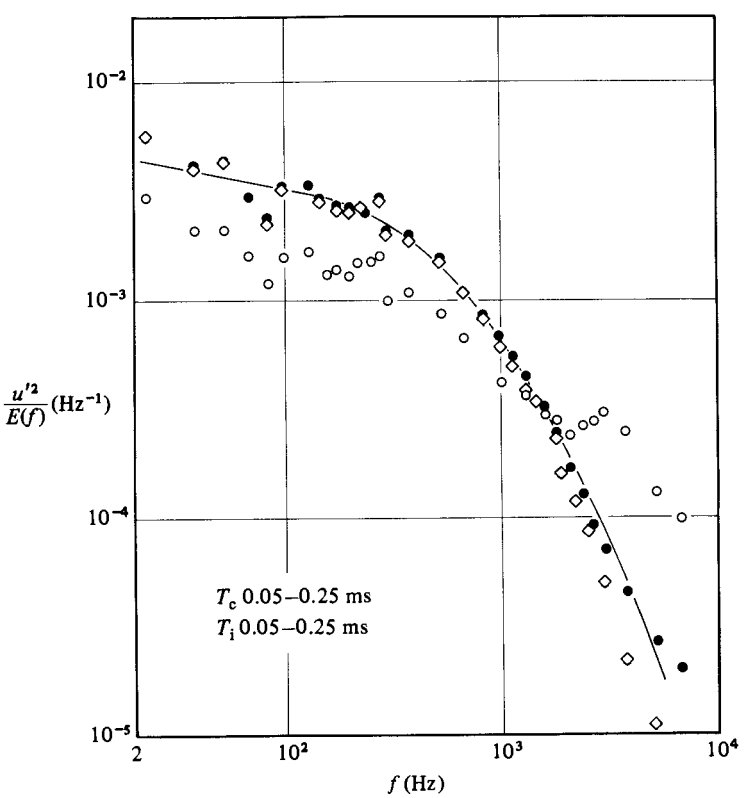

FIGURE 15. Frequency power spectrum of the simulation signal: ●, method (1); ○, method (2); ◇, method (3).

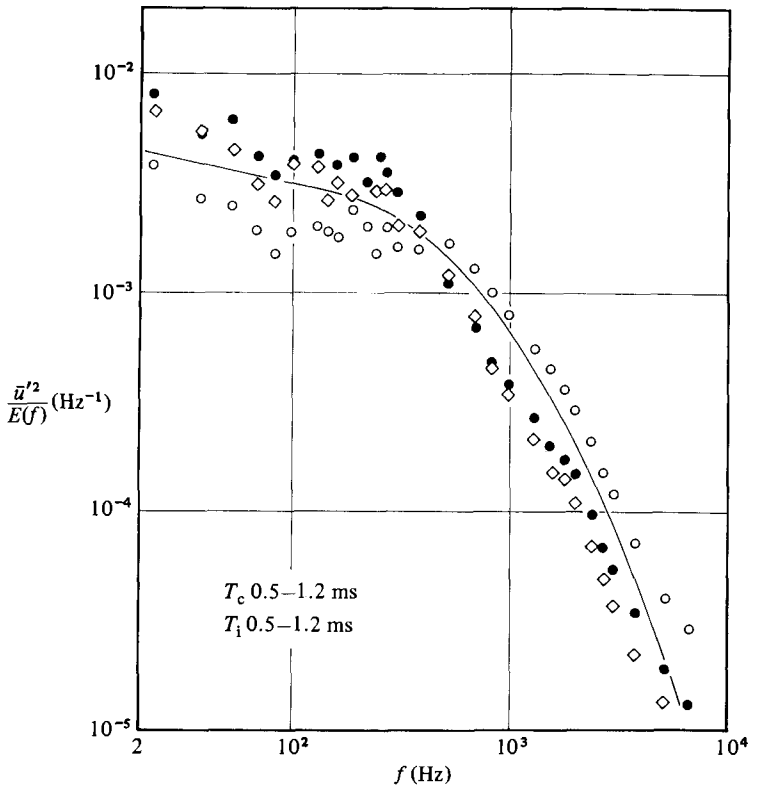

FIGURE 16. Frequency power spectrum of the simulation signal. For caption see figure 15.

increases further and reaches almost the same value as in the single-phase flow. Such a minimum value of turbulence intensity was also observed by Maeda *et al.* (1980), who showed the turbulence intensities measured by a hot-wire probe. However, the loading ratio corresponding to the minimum intensity was 0.1–0.3 in their experiment, where 136 μm glass beads were used. The loading ratio of the minimum intensity is abut 1.5 in the present experiment. The results of our previous work (Tsuji & Morikawa 1982) showed asymmetric distributions of mean and turbulent velocities because the pipe was set up horizontally, but there are similarities between the previous and present works in many respects. For instance, large particles promote turbulence, while small particles reduce it. Of course the particle density is also an important factor. For example, Lee & Durst (1982) showed that 800 μm glass beads (ρ_s = 2600 kg/m^3) increase turbulence for the entire region in the section, which is similar to the present case of 3 mm particles with density of 1000 kg/m^3.

Suppression of turbulence was shown in a liquid–solid two-phase flow by Zisselmar & Molerus (1979). The difference between the present and their results is that there exists a loading ratio giving the maximum turbulence intensity in their experiment, contrary to the minimum intensity in the gas–solid flow.

3.3. *Frequency spectrum of air turbulence*

In the present experiment, the signals from the frequency tracker were separated into the parts corresponding to large particles and those corresponding to small tracers for air flow. The presence of large particles interrupts signals of air flow, so that many

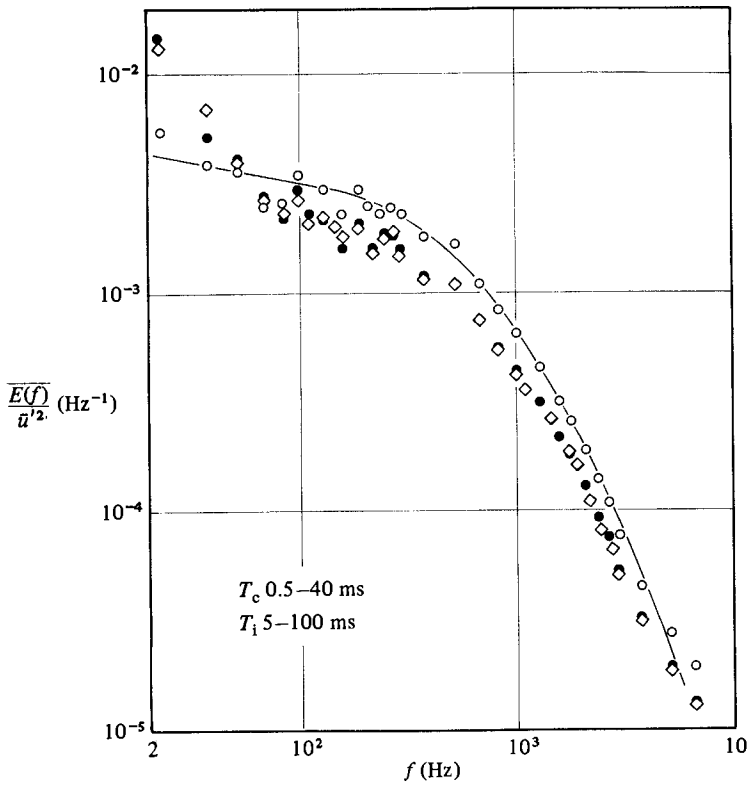

FIGURE 17. Frequency power spectrum of the simulation signal. For caption see figure 15.

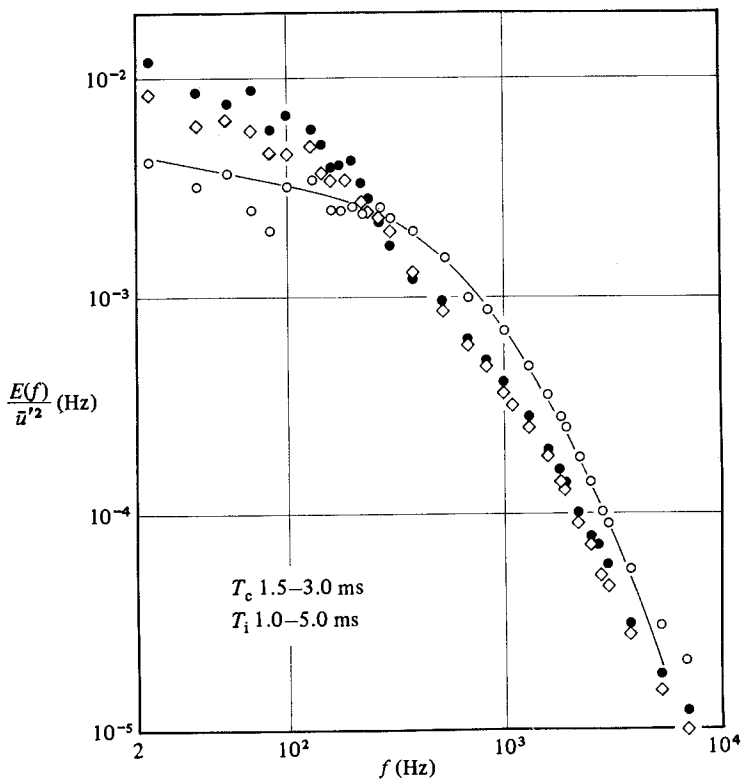

FIGURE 18. Frequency power spectrum of the simulation signal. For caption see figure 15.

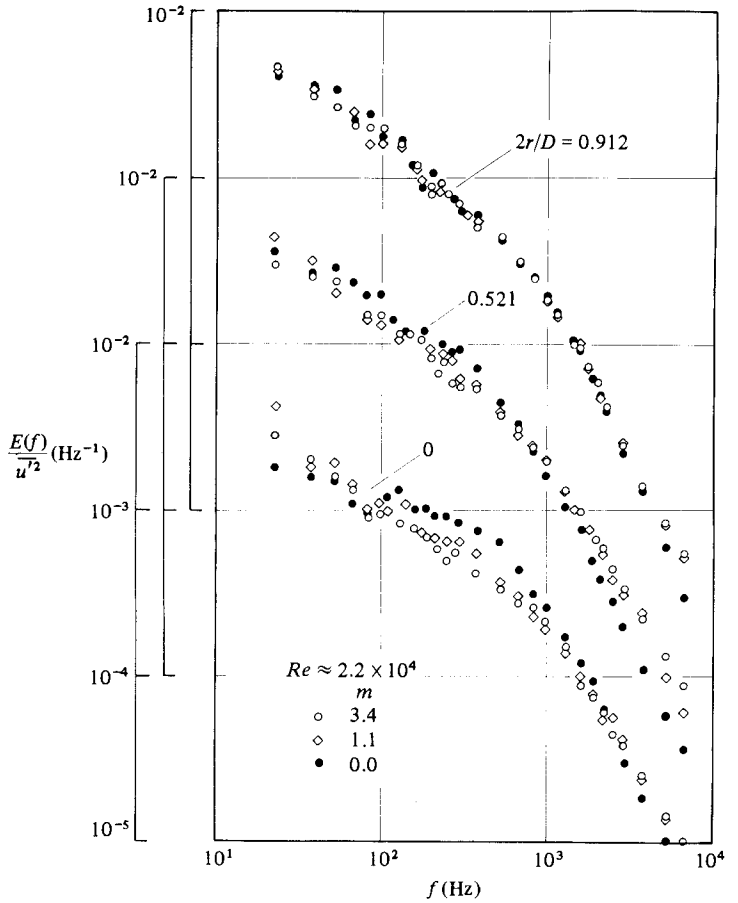

FIGURE 19. Frequency power spectrum of air turbulence in the presence of 3 mm particles.

defects are inevitable. Such defective parts are inconvenient in calculating the spectrum of turbulence. We have consistently adopted the FFT (fast Fourier transform) technique to obtain the spectrum, because FFT reduces the computing time greatly. However, in order to apply FFT to the present case, the defective parts should be interpolated suitably. In our previous work (Tsuji & Morikawa 1982), signals simulating two-phase flow were made artificially by imposing many defective parts on continuous signals of which spectrum was known, and suitable interpolation schemes were sought by trial. Figure 14 shows such interpolation methods that were examined. The signal A in the figure is the simulation signal with defective parts given artificially. The spectrum of the original signal without defect is known. The first interpolation (1) is to hold the value before the defect, the second is to replace defective parts by the average value, which is zero for the alternating component, and the third is to replace the defective part by a straight line connecting surviving parts. The third was suitable for the defect caused by 0.2 mm particles in our previous experiment (Tsuji & Morikawa 1982). However, it was found in this work that the third interpolation is not suitable for long defective parts. This means that the interpolation method must be selected according to the length of defect. Several sizes of particles were used in this experiment and each caused defects with different lengths. Unfortunately, there is not a general rule of interpolation for variable defects. Therefore the interpolation methods shown in figure 14 were again examined

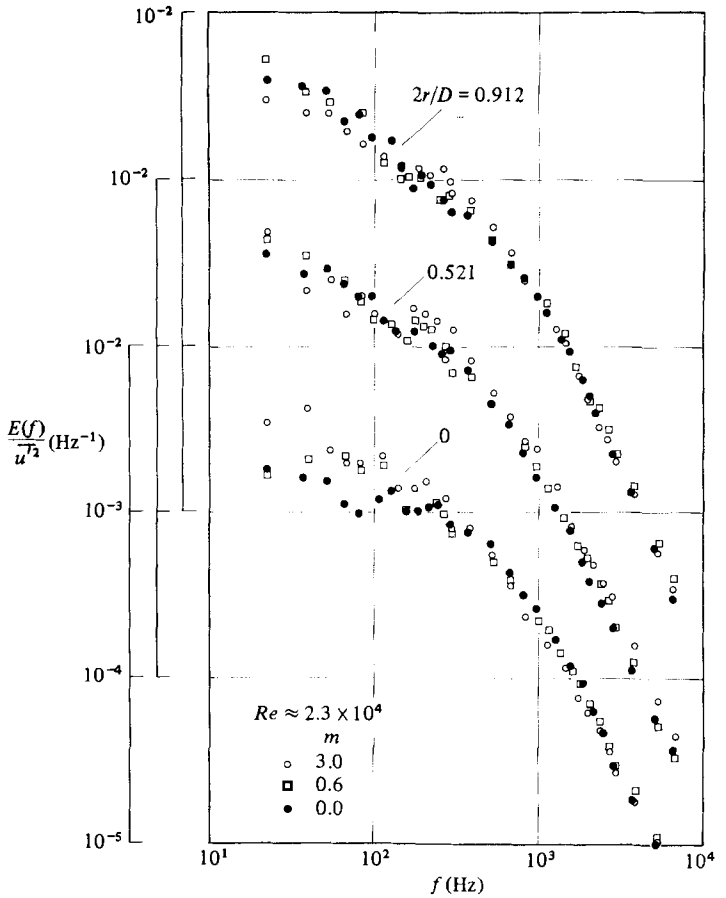

FIGURE 20. Frequency power spectrum of air turbulence in the presence of 1 mm particles.

systematically for simulated signals for various lengths of defect. The spectra calculated by using the interpolation methods (1)–(3) are compared in figure 15, where T_c and T_i are respectively the time interval and length of the defect occurrences. The solid line in the figure represents the spectrum of the original signal without defect, which is supposed to be the true spectrum. Ranges of T_c and T_i in figure 15 correspond to the defect caused by 0.2 mm particles. Figure 15 clearly indicates that the spectrum based on method (2) differs from the true one (solid line), while those based on methods (1) and (3) give satisfactory results. Figure 16 shows the results where T_c and T_i take larger values than those in figure 15. The error of the method observed in figure 15 is much reduced in figure 16. Cases of further large values of T_c and T_i are shown in figures 17 and 18, where method (2) gives us the most satisfactory results. Referring to the results shown above, we decided to adopt method (2) for defective parts longer than 1 ms and method (3) for those less than 1 ms, regardless of the size of particles. The calculation using method (3) tends to estimate the higher-frequency component to be a little less than the true value as shown in figure 15.

Figures 19–22 show the spectra of air turbulence in the presence of particles, which are normalized by the turbulence energy $\overline{u'^2}$. The spectra without particles are given for comparison. The difference between the single- and two-phase flows is small for relatively large particles like 3 and 1 mm particles. It is found that the presence of particles affects the spectra for 500 and 200 μm particles. Defective parts caused by

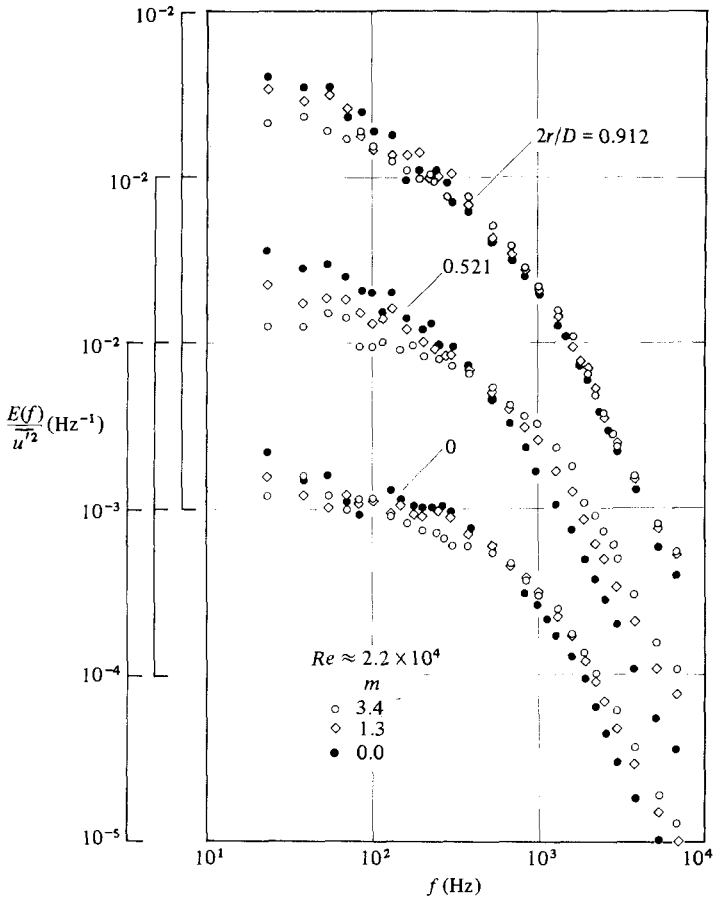

FIGURE 21. Frequency power spectrum of air turbulence in the presence of 500 μm particles.

small particles are interpolated mostly by method (3), which tends to underestimate the high-frequency part. In spite of this tendency, an increase in the high-frequency part is shown in figures 21 and 22. Therefore we can accept the above results more confidently. Tsuji & Morikawa (1982) obtained qualitatively the same results in a horizontal pipe. Baw & Peskin (1971) obtained the theoretical spectrum of fluid turbulence in the presence of particles. They showed that the high-frequency part was reduced by the particles, which is contrary to the present result. However, direct comparison of the present experiment with their theory is difficult, because several assumptions they used cannot be applied to the present case; for example, Stokes law for the fluid drag on the particle and isotropy of the turbulence.

Finally, we will discuss the microscales of turbulence and compare them with the particle size. Two kinds of microscale are commonly known, Taylor's microscale l_T and Kolmogoroff's one l_K, which are defined as

$$l_T = 15\nu \frac{\overline{u'^2}}{\epsilon}, \tag{1}$$

$$l_K = \left(\frac{\nu^3}{\epsilon}\right)^{\frac{1}{4}}, \tag{2}$$

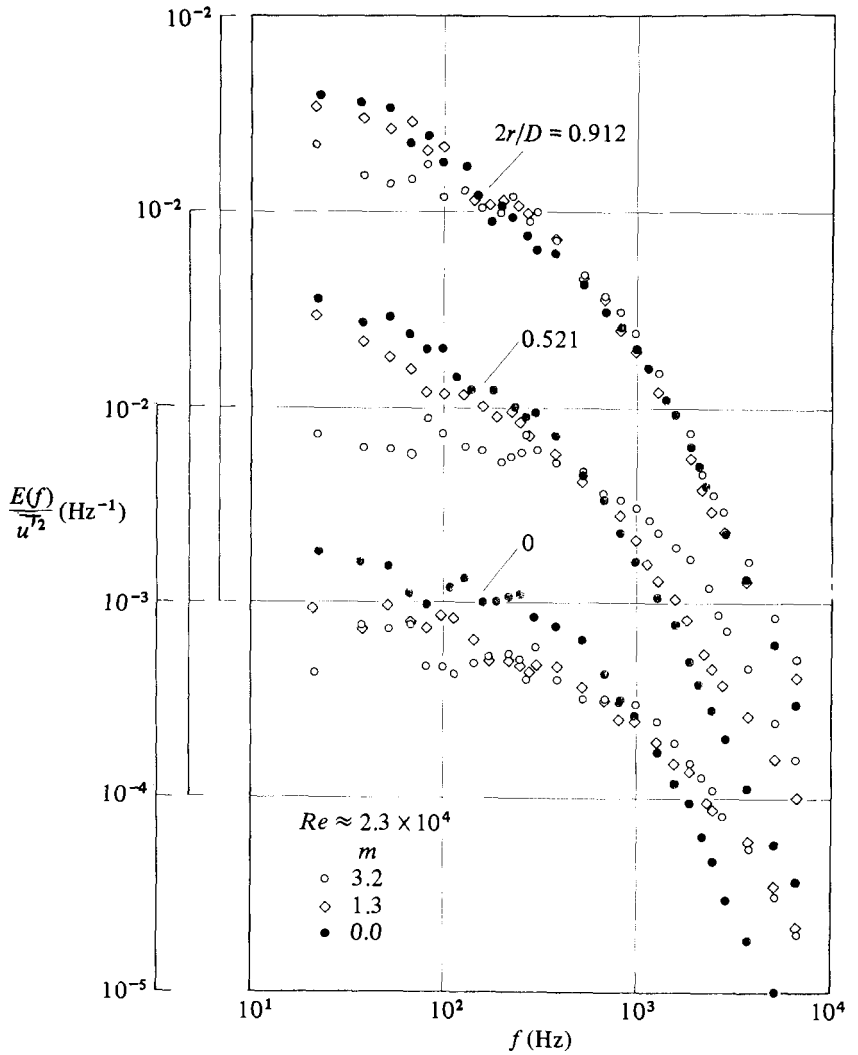

FIGURE 22. Frequency power spectrum of air turbulence in the presence of 200 μm particles.

where ϵ is the viscous dissipation of turbulent energy $\overline{u'^2}$. Afzal (1982) gave an empirical expression for ϵ:

$$\epsilon = \frac{u_\tau^3}{R}\left(\frac{2.44}{y/R} - 0.24\right), \tag{3}$$

where y is the distance from the wall and R is the pipe radius. The friction velocity $u_\tau = (\tau_w/\rho)^{\frac{1}{2}}$ is obtained from the pressure drop. The scales l_T and l_K are estimated by substituting (3) into (1) and (2). In the flow without particles, Taylor's scale l_T took the value of about 1.5 mm at the pipe centre, while Kolmogoroff's scale was about 50 μm near the wall and 100 μm at the pipe centre. The size of particles used in the present experiment is around the Taylor scale and larger than the Kolmogoroff scale.

REFERENCES

AFZAL, N. 1982 Fully developed turbulent flow in a pipe: an intermediate layer. *Ing. Arch.* **52**, 355.

BAW, P. S. H. & PESKIN, R. L. 1971 Some aspect of gas–solid suspension turbulence. *Trans. ASME* D: *J. Basic Engng* **93**, 631.

LEE, S. L. & DURST, F. 1982 On the motion of particles in turbulent duct flows. *Intl J. Multiphase Flow* **8**, 125.

MAEDA, M., HISHIDA, K. & FURUTANI, T. 1980 Optical measurements of local gas and particle velocity in an upward flowing dilute gas–solids suspension. *Proc. Polyphase Flow and Transport Technology* (*Century* 2-*ETC*, *San Francisco*), pp. 211.

TSUJI, Y. & MORIKAWA, Y. 1982 LDV measurements of an air–solid two phase flow in a horizontal pipe. *J. Fluid Mech.* **120**, 385.

VOLLHEIM, R. 1963 Verhalten der Wandschubspannung des Fördermediums beim pneumatischen Transport und Schlußfolgerungen für den Wärmeübergang. *Maschinenbautech.* **12**, 233.

ZISSELMAR, R. & MOLERUS, O. 1979 Experimentelle Untersuchungen zum Turbulenzverhalten der Suspensionsströmung in horizontalen Rohrleitungen. *Chem.-Ing.-Tech.* MS 656/79, 656.